Obtaining granular activated carbon from paper mill sludge – a challenge for application in the removal of pharmaceuticals from wastewater

Guilaine Jaria[1], Vânia Calisto[1*], Carla Patrícia Silva[1], María Victoria Gil[2], Marta Otero[3], Valdemar I. Esteves[1]

[1]Department of Chemistry & CESAM, University of Aveiro, Campus de Santiago, 3810-193 Aveiro, Portugal

[2]Instituto Nacional del Carbón, INCAR-CSIC, Calle Francisco Pintado Fe 26, 33011 Oviedo, Spain

[3]Department of Environment and Planning & CESAM, University of Aveiro, Campus de Santiago, 3810-193 Aveiro, Portugal

[*]corresponding author: vania.calisto@ua.pt

Abstract

In this work, a granular activated carbon (GAC) was produced using primary paper mill sludge (PS) as raw material and ammonium lignosulfonate (AL) as binder agent. PS is a residue from the pulp and paper industry and AL is a by-product of the cellulose pulp manufacture and the proposed production scheme contributes for their valorisation together with important savings in GAC precursors. The produced GAC (named PSA-PA) and a commercially available GAC (GACN), used as reference material, were physically and chemically characterized. Then, they were tested in batch experiments for the adsorption of carbamazepine (CBZ), sulfamethoxazole (SMX), and paroxetine (PAR) from ultra-pure water and wastewater. Even though GACN and PSA-PA possess very similar specific surface areas (S_{BET}) (629 and 671 m^2 g^{-1}, respectively), PSA-PA displayed lower maximum adsorption capacities (q_m) than GACN for the pharmaceuticals here studied (6 ± 1 - 44 ± 5 mg g^{-1} and 49 ± 6 - 106 ± 40 mg g^{-1}, respectively). This may be related to the comparatively higher incidence of mesopores in GACN, which might have positively influenced its adsorptive performance. Moreover, the highest hydrophobic character and degree of aromaticity of GACN could also have contributed to its adsorption capacity. On the other hand, the performance of both GACs was significantly affected by the matrix in the case of CBZ and SMX, with lower q_m in wastewater than in ultra-pure water. However, the adsorption of PAR was not affected by the matrix. Electrostatic interactions and pH effects might also have influenced the adsorption of the pharmaceutical compounds in wastewater.

Keywords: Industrial wastes, Waste management, Chemical activation, Agglomeration, Adsorptive water treatment, Emerging contaminants

1. Introduction

Activated carbons (ACs) are carbonaceous materials with high adsorption capacity towards a vast number of organic and inorganic compounds, such as pharmaceuticals, pesticides, personal care products, dyes and metals (Rodriguez-Narvaez et al., 2017). Commercial ACs, which are commonly produced from wood or coal (bituminous and sub-bituminous varieties), are available in powdered (PAC) or granular (GAC) formulations (Bandosz, 2006). GAC and PAC are used in water treatment, both presenting advantageous features and drawbacks depending on specific applications. PAC has the main advantage of, generally, possessing higher specific surface area (S_{BET}); however, it is usually applied in batch mode (due to inadequate particle size to be used in fixed-bed columns and difficult separation from the treated water in continuously stirred reactors). In the case of GAC, main advantages include its regeneration capability by thermal or chemical treatment and, therefore, its reuse, and the easiness of application in continuous mode, increasing the applicability in water treatment systems (Marsh and Rodríguez-Reinoso, 2006). The use of AC for the removal of organic contaminants from water, namely pharmaceuticals, is highly documented (e.g. Wang and Wang, 2016; Yang et al., 2017). Both PAC and GAC possess a great potential for the adsorption of these contaminants; yet, the use of PAC in wastewater treatment is usually associated to increased implementation and application costs and so GAC is generally the preferred option (Yang et al., 2017).

The production of AC from wastes has been proposed as an innovative and sustainable strategy (Silva et al., 2018), in line with an increasingly rigorous environmental legislation on the waste management that discourages disposal practices such as landfilling and incineration (European Commission, 2016 - Directive 2008/98/EC). Primary paper mill sludge (PS) is produced in large amounts, resulting from wastewater treatment in the

pulp and paper industry, so constituting an important waste management issue within this sector. Therefore, the use of PS to produce an added-value material such as AC can be considered as a valuable circular economy option, aligned with the challenges of this industry. Simultaneously, the use of PS as AC precursor has also proved to be advantageous since its characteristics present low variability throughout time, pointing out to its consistency to be used as raw material (Jaria et al., 2017). PAC produced from PS has already been used for the removal of pharmaceuticals from water, presenting similar or even higher adsorptive capacities than a commercial PAC (Jaria et al., *in press*). However, due to the fibrous and brittle structure of PS (mostly constituted by cellulose), attempts to use wastes with similar constitution to produce GAC have failed. In fact, a main problem of waste-derived GACs is usually the low attrition resistance of the produced materials, which may inhibit their use in adsorption beds (Smith et al., 2012). Different strategies have already been proposed to produce hardened GACs with high attrition resistance, being pelletization and/or the utilization of binder agents the most commonly used. The introduction of a pelletization step is usually the approach when the AC is produced by physical activation while the utilization of binders is usually the strategy in the case of chemical activation (Carvalho et al., 2006). Several patents have been published on the production of GAC employing binders such as urea-lignosulfonate (Blackmore, 1988) or ammonium lignosulfonate (Kovach, 1975). Also, in the scientific literature, the utilization of binders like humic acids (Lozano-Castelló et al., 2002) or clays (Carvalho et al., 2006) has been proposed. A comparison of different binders was carried out by Lozano-Castelló et al. (2002), who used a humic acid derived sodium salt, polyvinyl alcohol, a phenolic resin, Teflon and an adhesive cellulose-based binder for the preparation of AC monoliths. Also, Smith et al. (2012) compared the utilization of ammonium lignosulphonate, polyvinyl

alcohol, phenolic resin, araldite resin, lignosulphonic acid, calcium salt, and carboxymethyl cellulose sodium salt for the production of GACs from sewage sludge. The authors of both studies (Lozano-Castelló et al., 2002; Smith et al., 2012) highlighted the importance of selecting an appropriate binder so to avoid the deterioration of the adsorption performance of the final material.

In the above described context, this work aimed to give a step forward in the production of AC from PS and take on the challenge of obtaining, for the very first time, a cellulosic waste-based GAC to be used in the removal of pharmaceuticals from water. For the production of GAC, ammonium lignosulfonate (AL), which is a by-product derived from the sulphite process applied in the manufacture of cellulose pulp, was used as binder agent. The physicochemical characterization of the obtained GAC (PSA-PA) and of a commercial GAC (GACN, results of which are taken as reference), was performed and both adsorbents were tested under batch operation conditions for the adsorption of pharmaceuticals from ultra-pure water and also from wastewater. The versatility of the produced GAC was tested by studying the uptake of three pharmaceuticals from different therapeutic classes and with different physicochemical properties: the antiepileptic carbamazepine (CBZ), the antibiotic sulfamethoxazole (SMX), and the antidepressant paroxetine (PAR).

2. Materials and Methods

2.1. Reagents

AL was used as binder agent and was kindly provided by Rayonier Advanced Materials. KOH (EKA PELLETS, ≥86%) was used as chemical activating agent. For the washing step, HCl (AnalaR NORMAPUR, 37%) was used. The pharmaceuticals studied in

121 the adsorption tests were CBZ (Sigma Aldrich, 99%), SMX (TCI, >98%) and PAR
122 (paroxetine-hydrochloride, TCI, >98%). These pharmaceuticals belong to three different
123 therapeutic classes (anticonvulsants, antibiotics and antidepressants, respectively) and
124 present different physicochemical properties (depicted in Table S1 in Supplementary
125 Material (SM)). The GAC used as reference (GACN, DARCO 12×20, particle size between
126 0.8 and 1 mm) was kindly provided by Norit.
127 All the solutions were prepared in ultra-pure water obtained from a Milli-Q
128 Millipore system (Milli-Q plus 185) or in wastewater (details on sampling and
129 characterization are presented in section 2.4).
130
131 *2.2. Production of GAC from PS*
132 For the production of a GAC using PS as raw material, several experimental
133 approaches were tested until obtaining a material with suitable hardness to withstand the
134 target application. In this context, the following factors were tested: type of activating
135 agent; impregnation ratio between the precursor, the activating agent and the binder agent;
136 impregnation order (activating agent followed by the binder agent or *vice versa*); and one-
137 or two-step pyrolysis (detailed procedures are shown in Table 1). The optimized production
138 methodology was achieved by a two-stage process (test N in Table 1). All the other tested
139 conditions failed to produce a granular material. Accordingly, in the first stage, 30 g of PS
140 was mixed with 70 mL of AL aqueous solution (at 35%), resulting in a final PS:AL ratio
141 (*w/w*) of 6:5. The mixture was stirred overnight in a head-over-head shaker (80 rpm) and
142 left drying at room temperature followed by overnight oven-drying at 105 ºC. The dried
143 mixture was pyrolysed under inert atmosphere (N_2) at 500 ºC for 10 min. In a second stage,
144 each 10 g of the resultant carbon (named PSA) was activated with 20 mL of a solution of

KOH (at 50%), resulting in a PSA:KOH final ratio (*w/w*) of 1:1. The mixture was stirred for 1 h in an ultrasonic bath and oven-dried at 105 ºC overnight. This material was then pyrolysed at 800 ºC for 150 min, then washed with 1.2 M HCl and finally rinsed with distilled water until neutral pH was reached. The final GAC, named PSA-PA, was crushed, grounded and sieved to obtain a particle diameter between 0.5 and 1.0 mm.

2.3. Physicochemical characterization of PSA-PA and GACN

The physicochemical analysis of PSA-PA and GACN was performed by means of the determination of the total organic carbon (TOC) and inorganic carbon (IC); proximate and ultimate analyses; S_{BET} and Hg porosimetry; determination of the surface functionality by Boehm's titration; determination of the point of zero charge (pH_{pzc}); Fourier Transform Infrared Spectroscopy with Attenuated Total Reflectance (FTIR-ATR); X-Ray Photoelectron Spectroscopy (XPS) and Scanning Electron Microscopy (SEM). Detailed procedures are explained in section 2 of SM.

2.4 Wastewater sampling

The performance of PSA-PA and GACN was evaluated in a real wastewater matrix for the three considered pharmaceuticals. Wastewater samples were collected between May 2017 and January 2018 (5 sampling campaigns) at a local sewage treatment plant (STP) that treats domestic sewage (average daily flow of 39 278 m^3 day^{-1}; designed to serve 159 700 population equivalents). The STP operates both primary and biological treatments and the collected wastewater samples corresponded to the final treated effluent (after secondary decanting), which is discharged into the aquatic environment. After collection,

168 wastewater samples were filtered through 0.45 μm, 293 mm membrane filters (Gelman
169 Sciences), stored at 4 °C until analysis and used within no longer than 15 days.
170 Wastewater samples were characterized by measuring conductivity (WTW meter),
171 pH (pH/mV/°C meter pHenomenal® pH 1100L, VWR) and TOC (Shimadzu, model TOC-
172 V_{CPH}, SSM-5000A). The properties of wastewater samples used in this work are presented
173 in section 3 of SM.
174
175 *2.5. Batch adsorption experiments with PSA-PA and GACN*
176 Kinetic and equilibrium batch experiments were performed to determine the
177 adsorption of CBZ, SMX and PAR onto PSA-PA and GACN. For each pharmaceutical,
178 solutions with a known initial concentration were prepared in both ultra-pure water and
179 wastewater and stirred together with PSA-PA or GACN in an overhead shaker (Heidolph,
180 Reax 2) at 80 rpm and under controlled temperature (25.0 ± 0.1 ºC). After stirring,
181 solutions' aliquots were filtered through 0.22 μm PVDF filters (Whatman) and then
182 analysed for the remaining concentration of pharmaceutical. For all the initial
183 concentrations and pharmaceuticals, controls (containing the pharmaceutical solution, but
184 not GAC) were run simultaneously with experiments, which were carried out in triplicate.
185 The solutions were analysed by Micellar Electrokinetic Chromatography (MEKC) using a
186 Beckman P/ACE MDQ instrument (Fullerton, CA, USA), equipped with a photodiode
187 array detection system, according to the procedure described by Calisto et al. (2015).
188 Briefly, a dynamically coated silica capillary with 40 cm (30 cm to the detection window)
189 was used and the electrophoretic separation was accomplished at 25 ºC, in direct polarity
190 mode at 25 kV, during 5 min runs. Ethylvanillin was used as internal standard and sodium
191 tetraborate was used to obtain better peak shape and resolution and higher repeatability,

192 both spiked to all samples and standard solutions at final concentrations of 3.34 mg L^{-1} and
193 10 mM, respectively. Detection was monitored at 214 nm for CBZ and at 200 nm for SMX
194 and PAR. Separation buffer consisted of 15 mM of sodium tetraborate and 30 mM of
195 sodium dodecyl sulfate. All the analyses were performed in triplicate.

196 For the kinetic studies, a predefined mass of each GAC was placed in polypropylene
197 tubes and put in contact with 40 mL of a 5 mg L^{-1} aqueous single solution of each
198 pharmaceutical. The concentrations of both PSA-PA and GACN were: in ultra-pure water,
199 70 mg L^{-1} for CBZ, 50 mg L^{-1} for SMX, and 80 mg L^{-1} for PAR; in wastewater, 150 mg L^{-1}
200 for CBZ and PAR, and 200 mg L^{-1} for SMX. The solutions were shaken for different time
201 intervals between 0.5 and 72 h. The adsorbed concentration of pharmaceutical onto each
202 GAC at time *t*, q_t (mg g^{-1}), was calculated by Eq. 1:

203 $$q_t = \frac{(C_0 - C_t)V}{m} \qquad (1)$$

204 where C_0 (mg L^{-1}) is the initial concentration of pharmaceutical, C_t (mg L^{-1}) is the
205 concentration of pharmaceutical in solution at time *t*, *V* (L) is the volume of solution and *m*
206 is the mass of adsorbent (g). The kinetic models used for fitting the experimental data are
207 presented in Table S3 (section 4 of SM); non-linear fittings were performed using
208 GraphPad Prism, version 5.

209 Equilibrium experiments were carried out to determine the adsorption isotherms,
210 which allow to conclude about the adsorption capacity of the adsorbents. Equilibrium tests
211 were performed by varying the initial concentration of the pharmaceutical and keeping the
212 adsorbent mass constant. Hence, 40 mL of single solutions of each pharmaceutical, with
213 concentrations varying between 5.0 and 0.5 mg L^{-1} (a minimum of 6 concentrations were
214 considered for each system), were added to a predefined mass of carbon. In ultra-pure

water, the concentrations of PSA-PA were 50, 40 and 60 mg L^{-1} for the adsorption of CBZ, SMX and PAR, respectively; and the concentrations of GACN were 50, 40 and 40 mg L^{-1} for the adsorption of CBZ, SMX and PAR, respectively. In wastewater, the PSA-PA concentrations were of 125, 150 and 100 mg L^{-1} for the adsorption of CBZ, SMX, and PAR, respectively, while 125, 150 and 80 mg L^{-1} of GACN were used for the adsorption of CBZ, SMX, and PAR, respectively.

The adsorbed concentration of each pharmaceutical onto each GAC at the equilibrium, q_e (mg g^{-1}) was calculated by Eq. 2:

$$q_e = \frac{(C_0 - C_e)V}{m} \qquad (2)$$

where C_e (mg L^{-1}) is the concentration of pharmaceutical in solution at the equilibrium and all the other variables are defined as in Eq. 1. The isotherm models used for describing the experimental results are presented in Table S4 (section 4 of SM); non-linear fittings were performed using GraphPad Prism, version 5.

3. Results

3.1. Physicochemical characterization of PSA-PA and GACN

3.1.1. Chemical characterization

PSA-PA and GACN present a high value of TOC, 72 ± 2% and 79.7 ± 0.8%, respectively, and a very low value of IC, 0.029 ± 0.003% and 0.0204 ± 0.0002%, respectively. Thus, the results obtained for TOC and IC were very similar for the produced and reference GACs. Comparing the values for PSA-PA with those for the precursor (TOC = 29 ± 1% and IC = 3.3 ± 0.2% (Jaria et al., 2017)), the increase in the TOC content of the produced carbon compared with the precursor is clear.

The results of proximate and ultimate analyses are presented in Table 2 and show that both materials possess a high content in fixed carbon (77 and 81% for PSA-PA and GACN, respectively). The percentage in heteroatoms is higher for PSA-PA, namely in oxygen (13 and 6% for PSA-PA and GACN, respectively). Also, the H/C ratio indicates that GACN possesses a higher degree of aromaticity (lower H/C ratio) than PSA-PA.

Regarding FTIR-ATR analysis, the spectra for PSA-PA and for GACN are depicted in Figure S1 (section 2 of SM). The spectrum of PSA-PA (Figure S1a) shows peaks at 1530 cm^{-1}, which is characteristic of aromatic compounds and can be also associated to secondary amide N–H and C–N bending (1560-1530 cm^{-1}) (Stuart, 2004). The bands at 1100 and 1180 cm^{-1} might be associated with secondary alcohols C–O stretch and the bands between 3800 and 3600 cm^{-1} can be assigned to alcohol/phenol O–H stretching (Coates, 2000; Stuart, 2004). GACN spectrum (Figure S1b) revealed a broad band at 1125 cm^{-1} and a band at 1530 cm^{-1}, which can be associated to secondary alcohols C–O stretch and to the aromaticity of the material, respectively. Bands at 3605 and 3720 cm^{-1} evidence the presence of alcohol/phenol O–H stretching (Coates, 2000).

The determination of the surface functional groups (Table 3) indicated that both GACs have an acidic nature. This was confirmed by the values of pH_{pzc} determined for PSA-PA and GACN (Table 3). Also, from results in Table 3, it is possible to infer that the oxygen atoms present in both GACs are likely present in the form of carboxyl (particularly for GACN) and phenol groups, with lower incidence of lactones.

To complement the surface functionality characterization, XPS analysis was performed and the results are presented in Table 4. The results showed that PSA-PA possesses a high amount of oxygen compared with GACN. In fact, the XPS data indicate contents of 74.76% of carbon, 17.32% of oxygen and 2.34% of nitrogen for PSA-PA, and

90.49% of carbon and 7.26% of oxygen for GACN. These results are coincident with those from the ultimate analysis (Table 2). By deconvolution of the C 1s region, the prevalence of graphitic C sp^2 is evident (especially for GACN), along with the presence of C–C sp^3 bonds associated to phenolic, alcoholic and etheric carbons at the edge of the graphene layer (especially for PSA-PA) (Nielsen et al., 2014; Velo-Gala et al., 2014). These results are coincident with the FTIR-ATR spectra, presenting bands characteristic of alcohols (between 3800 and 3600 cm^{-1}), mainly observed in PSA-PA spectrum. Peaks associated to carbonyl or quinones and to carboxyl or ether groups are present in relatively similar percentages for both GACs (peaks 3 and 4, respectively, for C 1s). These results do not seem to be in agreement with the Boehm's titration results, since in those the carboxylic groups are in greater amount, especially in the case of GACN. These differences can be due to the fact that XPS is a surface technique while Boehm's titration is a bulk technique. Both spectra also present a peak at 291 eV, which can be associated to C π-π^* transition (Velo-Gala et al., 2014). Concerning the O 1s spectra, PSA-PA presents a peak at 535.5 (peak 3) which may be attributed to chemisorbed oxygen (Velo-Gala et al., 2014). Also, it presents a peak at 531 eV which can be assigned to C=O bonding in quinones and carbonyl groups, and a peak around 533 eV assigned to oxygen atoms of hydroxyl groups and to lactones and anhydrides. These two peaks (at 531 and 533 eV) are likewise in the GACN XPS spectrum, which also presents a peak at 534.4 eV that may be associated to oxygen of carboxyl groups, which is coincident with the Boehm's titrations results.

For PSA-PA it was also performed the fitting of the peaks associated to N 1s. In fact, comparing the overall spectra of the two GACs (Figure S2 in section 2 of SM) it is possible to clearly observe a peak in the N 1s zone for PSA-PA, while for GACN this peak is not noticeable. This is consistent with the higher N content of PSA-PA in comparison

with GACN, as revealed by the ultimate analysis (Table 2). The fitting indicates the presence of two peaks, at 398.0 and 400.1 eV, which might be attributed to pyridinic and pyrrolic N, respectively (Li et al., 2014; Wei et al., 2016).

3.1.2. Physical characterization

For the study of the textural features of the materials, nitrogen adsorption isotherms and SEM were used as characterization techniques. The results of S_{BET} and Hg porosimetry are presented in Table 5. For both GACs, S_{BET} and micropore volume (W_0) values are very similar; however, GACN possesses larger total pore volume (V_p) and average pore diameter (D) values than PSA-PA, which might have important implications in the adsorptive performance of the materials, as explained below (see section 3.2). Observing the pore size distribution (Figure 1), it is evident that PSA-PA possesses a narrower pore size distribution with prevalence of pores with 5 nm of diameter and smaller, whilst GACN presents a broader distribution, including a significant amount of larger pore sizes in the mesopores' range (2-50 nm). This may be an interesting feature of PSA-PA considering the selective adsorption of molecules with different sizes. On the other hand, the apparent density is similar for both materials, although it is slightly superior in the case of GACN.

The surface morphological structure of the two GACs was analysed by SEM (Figure 2). It is interesting to observe that, at the lowest magnifications, GACN appears to have a more homogeneous morphology but, at higher magnifications, the structure becomes rougher and the porosity is revealed. In the case of PSA-PA, at the lowest magnifications, a more disordered structure (possibly due to fragments of fibres that have not been destroyed) can be observed, but at higher magnification, porosity is also clearly observed.

3.2. Batch adsorption experiments with PSA-PA and GACN

3.2.1 Kinetic studies

The graphical representation of experimental and model results, and the parameters of the fitted models for the adsorption kinetics of CBZ, SMX and PAR onto the two studied GACs (PSA-PA and GACN) in ultra-pure water and in wastewater are presented in Figure 3 and Table 6, respectively. The kinetic models used to describe the adsorption experimental results were the pseudo-first order (PFO) and pseudo-second order (PSO) models (Table S3, section 4 in SM).

As it may be seen in Table 6, the fittings to the PFO and the PSO models presented R^2 values above 0.90, except for the adsorption kinetics of PAR onto GACN, in ultra-pure water. Therefore, both models (PFO and PSO) were considered to reasonably describe the experimental data. In general terms, it may be said that, for CBZ and SMX, the results were slightly better described by the PSO model, while PFO model was the most adequate to describe the adsorption kinetics of PAR.

In relation to the rate constants k_1 and k_2, the values vary between 10^{-6} and 10^{-3} (min^{-1} or g mg^{-1} min^{-1}, respectively). These low values are in agreement with the relatively long equilibrium times (above 24 h) here determined. It must be taken into account that, due to the particle size of GACs, adsorption kinetics are usually slower than onto powdered materials. Nevertheless, it is possible to observe that GACN presents a slightly faster adsorption rate than PSA-PA for CBZ in ultra-pure water (2 times higher k_2), and for PAR in ultra-pure and wastewater (3.6 and 3.25 times higher k_1, respectively), while PSA-PA presents a faster adsorption rate than GACN in the case of CBZ in wastewater (4 times

333 higher k_2) and SMX in both matrices (3.5 times higher k_2 in ultra-pure water and 22 times
334 higher k_2 in wastewater).

335 *3.2.2. Equilibrium studies*

336 Experimental equilibrium and model results, and the corresponding parameters of
337 the non-linear fittings, for the adsorption of CBZ, SMX and PAR onto PSA-PA and GACN
338 in ultra-pure water and in wastewater are presented in Figure 4 and Table 6, respectively.
339 The isotherm models used to describe the equilibrium experimental results were Langmuir,
340 Freundlich and Sips models (Table S4, section 4 in SM).

341 Equilibrium results of the three pharmaceuticals onto PSA-PA, either in ultra-pure
342 or wastewater, were better described by the Langmuir and the Sips models than by the
343 Freundlich model. In the case of GACN, the Sips model revealed to be not suitable to
344 model the experimental data, with most of the fittings being ambiguous. Considering the
345 other tested models, even though the Freundlich equation has presented fittings with R^2
346 values slightly higher in some cases, it can be said that the equilibrium results were mostly
347 best fitted by the Langmuir isotherm. Thus, to allow the comparison of the results of all the
348 studied systems, the Langmuir model was selected.

349 The Langmuir maximum adsorption capacity (q_m) of GACN is higher than that of
350 PSA-PA. For the latter, q_m values range from 24 ± 5 to 44 ± 5 mg g^{-1} and from 6 ± 1 to 34 ±
351 9 mg g^{-1}, in ultra-pure water and wastewater, respectively. Meanwhile, for GACN, the q_m
352 range from 64 ± 12 to 98 ± 17 mg g^{-1} and from 49 ± 6 to 106 ± 40 mg g^{-1}, in ultra-pure
353 water and wastewater, respectively. Both GACs present better performance for CBZ and
354 SMX in ultra-pure water than in wastewater. However, the effect of the aqueous matrix in
355 q_m was not remarkable for the adsorption of PAR, particularly in the case of PSA-PA.

As it may be seen in Figure 4, the adsorption of CBZ onto GACN was much lower in wastewater than in ultra-pure water. The decrease was not so evident in the adsorption of CBZ onto PSA-PA, but, still, q_m decreased from 24 ± 5 mg g^{-1} (in ultra-pure water) to 10 ± 1 mg g^{-1} (in wastewater). The q_m determined for the adsorption of SMX onto both carbons in wastewater was lower than in ultra-pure water. However, while in the case of GACN the adsorption capacity decreased to a half (from 98 ± 17 to 49 ± 6 mg g^{-1}), the decrease was more accentuated for PSA-PA (from 44 ± 5 to 6 ± 1 mg g^{-1}). Finally, as evidenced in Figure 4 and confirmed by the parameters in Table 6, the adsorption of PAR onto both carbons remained mostly the same in wastewater and in ultra-pure water.

4. Discussion

Analysing the structural properties of both carbons (Table 5), it is possible to see that S_{BET} and W_0 are very similar, indicating that these parameters are probably not the main factors influencing the differences observed between the GACs with respect to the adsorption of the studied pharmaceuticals. However, V_p and D of GACN are significantly superior to those of PSA-PA. Taking into account the similar value of the W_0 for both GACs, a larger V_p in GACN indicates that this carbon has a higher presence of mesopores in its porous structure. Furthermore, the pore size distribution (Figure 1) clearly evidences that GACN has a broader distribution of the pore sizes in the range of mesopores (2-50 nm), while PSA-PA has a higher presence of pores below 5 nm. Therefore, the mesoporous character of the GACN could explain to a certain extent the better results of the adsorption experiments for this adsorbent. This might be due not only to the importance of mesopores as channels that guarantee the accessibility to micropores but also to the molecular sizes of the studied pharmaceuticals, which are very close to the PSA-PA average pore diameter

(between 0.653 and 1.174 nm for CBZ and between 0.623 and 1.362 nm for SMX (Nielsen et al., 2014)). The influence of these parameters in the adsorption of pharmaceuticals onto waste-based activated carbons has also been reported by Mestre et al. (2009). On the other hand, for PSA-PA, which possesses a higher amount of functional groups (Table 3), surface interactions are more likely to be present.

Considering the adsorption of CBZ, for both GACs and matrices, the compound is mainly in the neutral form (see pK_a values in Table S1, in section 1 of SM), which indicates that electrostatic forces do not play a significant role in the adsorption process. Also, CBZ has a low solubility in water at 25 ºC and a high log K_{ow} (Table S1, in section 1 of SM), and therefore, hydrophobic interactions may play an important role mainly in ultra-pure water. Considering that the adsorption of CBZ onto GACN is higher than in PSA-PA, GACN might be more hydrophobic than PSA-PA, since it possesses fewer surface functional groups and higher prevalence of graphitic carbon and thus a higher degree of aromaticity (Tables 2-4). In this context, and particularly for GACN, π–π interactions may occur between CBZ benzene rings (that act as a π–electron acceptor due to the amide functionality, which functions as an electron withdrawing group (Cai and Larese-Casanova, 2014)) and the aromatic benzene rings of the graphitic part of the carbon that can act as π–electron donor groups, forming a π– π electron donor-acceptor complex.

Relative to the adsorption of SMX and similarly to CBZ, π–π interactions can occur between the π-donor hydroxyl substituent groups of the benzene rings and the π-acceptor of SMX amino group and N-heteroaromatic rings (Zhang et al., 2010). This last interaction may have contributed, in part, to the higher adsorption capacity of SMX onto GACN, since according to the H/C ratio (Table 2) and as above referred, this carbon presents a higher degree of aromaticity and, therefore, of graphitic carbon (as confirmed by the XPS results

404 (Table 4)). The reduction of the adsorption capacity of the GACs towards SMX from ultra-
405 pure water to wastewater can be explained by the pH change, since in the case of the
406 wastewater matrix (pH between 7 and 8), both GACs present a negative net charge (pH_{pzc}
407 between 4 and 5) and SMX species are mostly present in the anionic form (see pK_a values
408 in Table S1, in section 1 of SM), and therefore, electrostatic repulsion is likely to occur.
409 Besides, SMX is the pharmaceutical possessing the lowest log K_{ow} value (see Table S1, in
410 section 1 of SM), being the less adsorbed pharmaceutical in this condition.
411 For the adsorption of PAR onto both GACs, no significant differences were verified
412 between adsorption capacities in ultra-pure water and wastewater (Figure 4). In fact, PAR
413 is mostly present in its positive form in both matrices (see pK_a values in Table S1, in
414 section 1 of SM) and thus, in the case of wastewater, electrostatic interactions have
415 certainly an important role in the adsorption process, balancing competitive effects that
416 may affect the carbons' adsorption capacity. Also, PAR possesses a high value of log K_{ow}
417 (see Table S1, in section 1 of SM), which is considered to positively influencing the
418 adsorption onto the nonpolar surface of activated carbons (Çeçen and Aktaş, 2011).
419 All the target pharmaceuticals possess hydrogen-bonding acceptors, namely, three H
420 bond acceptors in CBZ, four in PAR and six in SMX (Table S1, in section 1 of SM).
421 Analysing the q_m values for the three pharmaceuticals in ultra-pure water for PSA-PA, it is
422 possible to observe some correlation with the number of hydrogen-bonding acceptors as
423 PSA-PA shows a higher adsorption capacity for SMX (the pharmaceutical with higher
424 hydrogen bond acceptors), and a smaller adsorption capacity for CBZ (the one possessing
425 the lowest number of hydrogen bond acceptors). This can point out hydrogen bonding as
426 one of the possible mechanisms occurring in the adsorption of these pharmaceuticals in
427 ultra-pure water onto PSA-PA. This tendency, however, is not maintained in the

wastewater matrix, where the highest adsorption capacity is obtained for PAR, followed by CBZ, and SMX. Thus, as referred above, pH effects and electrostatic interactions appear to be important factors ruling the adsorption of the studied pharmaceuticals in wastewater.

5. Conclusions

In this work, fourteen different procedures were tested to accomplish the challenge of producing a GAC from an industrial waste. The production of a GAC was only possible using AL as binder agent and it was successfully achieved by a procedure involving a two-step pyrolysis. Then, the resulting material (PSA-PA) was applied for the adsorptive removal of CBZ, SMX and PAR from water. It was found that PSA-PA exhibits very similar physicochemical properties to a commercial GAC (GACN, used as reference) in what concerns S_{BET}, micropore volumes, predominance of surface phenol and carboxylic groups and acidic pH_{pzc}. However, PSA-PA possesses a total pore volume and an average pore diameter twice lower than GACN, indicating a significantly higher presence of mesopores in GACN, which may be responsible for the lower adsorption capacity of PSA-PA towards the considered pharmaceuticals. On the other hand, the adsorption capacity of PSA-PA and GACN was strongly affected by the matrix, with a significant decrease in the adsorption of CBZ and SMX from wastewater as compared with ultra-pure water. However, the same effect was not verified for the adsorption of PAR, which could be explained by pH effects and electrostatic interactions. Although PSA-PA showed lower adsorption capacities than GACN for ultra-pure water and wastewater tests, it should be considered that the produced adsorbent is a waste-based carbon, and other parameters apart from the maximum adsorption capacity (such as its dynamic behaviour and cost) need to be studied in detail in future works. For example, relatively fast adsorption rate for some of the studied cases was here verified, indicating the potential of PSA-PA. Overall, this study

452 represents a step forward in the utilization of PS as raw material for GAC production,
453 enabling its application in fixed-bed systems for the adsorption of pharmaceuticals, which
454 will be considered in future work of this research group.

455 *Acknowledgments*

456 This work was funded by FEDER through COMPETE 2020 and by national funds
457 through FCT by the research project PTDC/AAG-TEC/1762/2014. Vânia Calisto and
458 Marta Otero also thank FCT for a postdoctoral grant (SFRH/BPD/78645/2011) and support
459 by the FCT Investigator Program (IF/00314/2015), respectively. Thanks are also due for the
460 financial support to CESAM (UID/AMB/50017-POCI-01-0145-FEDER-007638), to
461 FCT/MCTES through national funds (PIDDAC), and the co-funding by the FEDER, within
462 the PT2020 Partnership Agreement and Compete 2020. Milton Fontes and workers of
463 Aveiro's STP (Águas do Centro Litoral) are gratefully acknowledged for assistance on the
464 effluent sampling campaigns. The authors also thank Rayonier Advanced Materials for
465 kindly providing the binder agent used in this work.

466

467 *References*

468 Aygün, A., Yenisoy-Karakas, S., Duman, I., 2003. Production of granular activated carbon from
469 fruit stones and nutshells and evaluation of their physical, chemical and adsorption properties.
470 Micropor Mesopor Mat 66, 189-195.
471 Bae, W., Kim, J., Chung, J., 2014. Production of granular activated carbon from food processing
472 wastes (walnut shells and jujube seeds) and its adsorptive properties. J Air Waste Ma 64, 879–886.
473 Bandosz, T.J., 2006. Activated Carbon Surfaces in Environmental Remediation, first
474 edition, Elsevier, New York.

475 Belhachemi, M., Addoun, F., 2011. Comparative adsorption isotherms and modeling of methylene
476 blue onto activated carbons. Applied Water Science 1, 111-117.
477 Blackmore, K.A.E., 1988. Lignosulfonate/urea binder for particulate composites. US Patent
478 4,786,438, filed August 10, 1987 and issued November 22, 1988.
479 Cai, N., Larese-Casanova, P., 2014. Sorption of carbamazepine by commercial graphene oxides: a
480 comparative study with granular activated carbon and multiwalled carbon nanotubes. J Colloid
481 Interf Sci 426, 152-161.
482 Calisto, V., Ferreira, C.I., Oliveira, J.A., Otero, M., Esteves, V.I., 2015. Adsorptive removal of
483 pharmaceuticals from water by commercial and waste-based carbons. J Environ Manage 152, 83-
484 90.
485 Carvalho, A.P., Mestre, A.S., Pires, J., Pinto, M.L., Rosa, M.E., 2006. Granular activated carbons
486 from powdered samples using clays as binders for the adsorption of organic vapours. Micropor
487 Mesopor Mat. 93, 226–231.
488 Çeçen, F., Aktaş, Ö., 2011. Integration of Activated Carbon Adsorption and Biological Processes in
489 Wastewater Treatment, in Activated Carbon for Water and Wastewater Treatment: Integration of
490 Adsorption and Biological Treatment. Wiley-VCH Verlag GmbH & Co. KGaA, Weinheim,
491 Germany.
492 Coates, J., 2000. Interpretation of Infrared Spectra - A Practical Approach, in: Encyclopedia of
493 Analytical Chemistry. John Wiley & Sons Ltd, Chichester.
494 Ebadi, A., Soltan Mohammadzadeh, J.S., Khudiev, A., 2009. What is the correct form of BET
495 isotherm for modeling liquid phase adsorption? Adsorption 15, 65-73.
496 European Commission, 2016. Directive 2008/98/EC on Waste (Waste Framework Directive).
497 http://ec.europa.eu/environment/waste/framework/ (Accessed on September 2018).
498 Foo, K.Y., Hameed, B.H., 2010. Insights into the modeling of adsorption isotherm systems. Chem
499 Eng J 156, 2-10.

Jaria, G., Silva, C.P., Ferreira, C.I., Otero, M., Calisto, V., 2017. Sludge from paper mill effluent treatment as raw material to produce carbon adsorbents: An alternative waste management strategy. J Environ Manage 188, 203-211.

Jaria, G., Silva, C.P., Oliveira, J.A.B.P., Santos, S.M., Gil, M. V, Otero, M., Calisto, V., Esteves, V.I., *In Press*. Production of highly efficient activated carbons from industrial wastes for the removal of pharmaceuticals from water-A full factorial design. J Hazard Mater.

Kim, J.-W., Sohn, M.-H., Kim, D.-S., Sohn, S.-M., Kwon, Y.-S., 2001. Production of granular activated carbon from waste walnut shell and its adsorption characteristics for Cu2+ ion. J Hazard Mater B 85, 301-315.

Kovach, J. L., 1975. Hard granular activated carbon and preparation from a carbonaceous material a binder and a inorganic activating agent. US Patent 3,864,277, filed August 14, 1972, and issued at February 4 1975.

Largitte, L., Pasquier, R., 2016. A review of the kinetics adsorption models and their application to the adsorption of lead by an activated carbon. Chemical Engineering Research and Design 109, 495-504.

Li, Z., Xu, Z., Wang, H., Ding, J., Zahiri, B., Holt, C.M.B., Tan, X., Mitlin, D., 2014. Colossal pseudocapacitance in a high functionality–high surface area carbon anode doubles the energy of an asymmetric supercapacitor. Energy Environ Sci 7, 1708–1718.

Liu, Y.a.S.L., 2008. From Langmuir Kinetics to First- and Second-Order Rate Equations for Adsorption. Langmuir 24, 11625-11630.

Lozano-Castelló, D., Cazorla-Amorós, D., Linares-Solano, A., Quinn, D.F., 2002. Activated carbon monoliths for methane storage: influence of binder. Carbon, 40, 2817–2825.

Marczewski, A.W., 2007. Kinetics and equilibrium of adsorption of organic solutes on mesoporous carbons. Appl Surf Sci 253, 5818-5826.

Markovic, D.D., Lekic, B.M., Rajakovic-Ognjanovic, V.N., Onjia, A.E., Rajakovic, L.V., 2014. A new approach in regression analysis for modeling adsorption isotherms. Sci World J 2014, 930879.

526 Marsh, H., Rodríguez-Reinoso, F., 2006. Activated Carbon, First ed. Elsevier, England.
527 Mestre, A.S., Pires, J., Nogueira, J.M.F., Parra, J.B., Carvalho, A.P., Ania, C.O., 2009. Waste-
528 derived activated carbons for removal of ibuprofen from solution: Role of surface chemistry and
529 pore structure. Bioresource Technol 100, 1720–1726.
530 Nielsen, L., Biggs, M.J., Skinner, W., Bandosz, T.J., 2014. The effects of activated carbon surface
531 features on the reactive adsorption of carbamazepine and sulfamethoxazole. Carbon 80, 419-432.
532 Pan, B.C., Xiong, Y., Su, Q., Li, A.M., Chen, J.L., Zhang, Q.X., 2003. Role of amination of a
533 polymeric adsorbent on phenol adsorption from aqueous solution. Chemosphere 51, 953-962.
534 Park, K.-H., Balathanigaimani, M.S., Shim, W.-G., Lee, J.-W., Moon, H., 2010. Adsorption
535 characteristics of phenol on novel corn grain-based activated carbons. Micropor Mesopor Mat 127,
536 1-8.
537 Qiu, H., Lv, L., Pan, B.-c., Zhang, Q.-j., Zhang, W.-m., Zhang, Q.-x., 2009. Critical review in
538 adsorption kinetic models. J Zhejiang Univ-SC A 10, 716-724.
539 Rodriguez-Narvaez, O.M., Peralta-Hernandez, J.M., Goonetilleke, A., Bandala, E.R., 2017.
540 Treatment technologies for emerging contaminants in water: A review. Chem Eng J 323, 361-380.
541 Silva, C.P., Jaria, G., Otero, M., Esteves, V.I., Calisto, V., 2018. Waste-based alternative adsorbents
542 for the remediation of pharmaceutical contaminated waters: Has a step forward already been taken?
543 Bioresource Technol 250, 888–901.
544 Smith, K.M., Fowler, G.D., Pullket, S., Graham, N.J.D., 2012. The production of attrition resistant,
545 sewage–sludge derived, granular activated carbon. Sep Purif Technol 98, 240–248.
546 Stuart, B., 2004. Infrared Spectroscopy : Fundamentals and Applications. Wiley, Chichester, West
547 Sussex, England.
548 Tan, K.L., Hameed, B.H., 2017. Insight into the adsorption kinetics models for the removal of
549 contaminants from aqueous solutions. J Taiwan Inst Chem E 74, 25-48.
550 Velo-Gala, I., López-Peñalver, J.J., Sánchez-Polo, M., Rivera-Utrilla, J., 2014. Surface
551 modifications of activated carbon by gamma irradiation. Carbon 67, 236–249.

552 Wang, J., Wang, S., 2016. Removal of pharmaceuticals and personal care products (PPCPs) from
553 wastewater: A review. J Environ Manage 182, 620-640.
554 Wei, T., Zhang, Q., Wei, X., Gao, Y., Li, H., 2016. A Facile and Low-Cost Route to Heteroatom
555 Doped Porous Carbon Derived from Broussonetia Papyrifera Bark with Excellent Supercapacitance
556 and CO_2 Capture Performance. Sci. Rep. 6, 22646.
557 Yang, R.T., 2003. Adsorbents: Fundamentals and Applications. John Wiley & Sons, Inc., New
558 Jersey.
559 Yang, Y., Ok, Y.S., Kim, K.H., Kwon, E.E., Tsang, Y.F., 2017. Occurrences and removal of
560 pharmaceuticals and personal care products (PPCPs) in drinking water and water/sewage treatment
561 plants: A review. Sci Total Environ 596-597, 303-320.
562 Zhang, D., Pan, B., Zhang, H., Ning, P., Xing, B., 2010. Contribution of Different
563 Sulfamethoxazole Species to Their Overall Adsorption on Functionalized Carbon Nanotubes.
564 Environ Sci Tech 44, 3806-3811.

Tables

Click here to download Table: tables_REVISED.docx

Table 1 – Experimental conditions tested for the production of a GAC using primary paper mill sludge (PS) as precursor, ammonium lignosulfonate (AL) as binder agent and different chemical activating agents (AA).

Test	Activating agent (AA)	Ratio (*w/w/w*)	Procedure
A	K_2CO_3	10:10:1[a]	AL was mixed in different proportions with PS and with the AA solution. It was left to dry and pyrolysed at 800 ºC for 150 min. From tests A to C, AL was added as an aqueous solution; from tests D to H, AL was added as a powder.
B	K_2CO_3	4:4:1[a]	
C	K_2CO_3	2:2:1[a]	
D	K_2CO_3	10:10:1[a]	
E	K_2CO_3	4:4:1[a]	
F	K_2CO_3	2:2:1[a]	
G	KOH	2:2:1[a]	
H	H_3PO_4	2:2:1[a]	
I	KOH	2:2:1[a]	PS was firstly washed with HCl 1.2 M and then with distilled water until neutral pH was reached, for the removal of ashes. Next, washed PS was mixed with AL (in powder) and AA, left to dry and pyrolysed at 800 ºC for 150 min.
J	KOH	2:2:1[a]	PS was mixed with AL (in solution) in an overhead shaker for 12 h. After drying at room temperature, it was added to AA, left to dry and pyrolysed at 800 ºC for 150 min.
K	KOH	2:2:1[a]	PS was mixed with AA and left to dry at room temperature. Next, AL (in solution) was added and the mixture was dried and pyrolysed at 800 ºC for 150 min.
L	K_2CO_3	2:2:1[a]	
M	K_2CO_3	6:5[b] and 1:1[c]	PS was mixed with the AL (in solution), dried and pyrolysed at 500 ºC for 10 min. The obtained carbon (PSA) was then mixed with the AA at a 1:1 ratio (PSA:AA, *w:w*). This mixture was shaken during 1 h in an ultrasonic bath, dried and pyrolysed at 800 ºC for 150 min. The final carbon (PSA-PA) was then washed with HCl 1.2 M and distilled water until neutral pH was reached.
N	KOH	6:5[b] and 1:1[c]	

[a]PS:AA:AL ratio; [b]PS:AL ratio; [c]PSA:AA ratio

Note: All the pyrolysis experiments were carried out under N_2 atmosphere.

Table 2 – Proximate and ultimate analyses for PSA-PA and GACN.

	PSA-PA	GACN
Proximate Analysis (db)		
Moisture (wt%)	8	8
Volatile Matter (wt%)	13	6
Fixed Carbon (FC)	77	81
Ash (wt%)	9	13
FC/VM	6	14
Ultimate Analysis (dab)		
%C	81.2	92.4
%H	1.9	0.75
%N	3.0	0.75
%S	0.80	0.05
%O	13.1	6.0
H/C	0.02	0.008
O/C	0.16	0.06
N/C	0.04	0.008

Notes:
Except for moisture, all values in proximate analysis are presented in a dry basis (*db*).
FC values were determined by difference.
Ultimate analysis is presented in a dry and ash free basis (*dab*).
The values of %O were estimated by difference: %O = 100% - (%C + %H + %N + %S).

Table 3 – Amount of acidic and total basic functional groups of PSA-PA and GACN determined by Boehm's titration.

Material	**Amount of functional groups (mmol g^{-1})**				**pH_{pzc}**
	Carboxylics	***Lactones***	***Phenols***	***Basic (total)***	
PSA-PA	1.29	0.29	0.96	0.31	4.3
GACN	1.03	0.02	0.31	0.34	4.8

Table 4 – X-ray photoelectron spectroscopy (XPS) results for PSA-PA and GACN.

		PSA-PA		GACN		Possible bond assignment
	Peak	**Binding Energy (eV)**	**%**	**Binding Energy (eV)**	**%**	
C 1s	1	284.5	58.5	284.6	68.4	C sp^2; graphitic carbon
	2	285.8	22.0	285.8	10.2	C-C sp^3; C-(O, N, H): phenolic, alcoholic, etheric carbon
	3	287.6	7.3	287	8.2	C=O: carbonyl or quinone
	4	289	6.3	288.9	5.4	O-C=O: carboxyl or ether
	5	291	5.9	291	7.7	π-π* transition in C
O 1s	1	531.1	20.1	531.2	24.4	C=O: carbonyl or quinone
	2	533	54.6	533	44.4	C=O: carboxyl/carbonyl or sulfoxides/sulfones; O-C: phenol/epoxy, ether, ester, anhydride, carboxyl
	3	-	-	534.4	22.0	-COOH or -COOR
		535.3	17.5	-	-	Water or chemisorbed oxygen
	4	537.6	7.7	536.5	9.2	Chemisorbed water
N 1s	1	398.0	18.9	-	-	Pyridinic N (N-6)
	2	400.1	81.9	-	-	Pyrrolic N (N-5)

Table 5– Textural characterization of PSA-PA and GACN.

Sample	**Apparent density, ρ_{Hg} (g cm^{-3})**	**N_2 adsorption at −196 °C**						
				Dubinin-Radushkevich (DR)			**Dubinin-Astakhov (DA)**	
		S_{BET} (m^2 g^{-1})	**V_p (cm^3 g^{-1})**	**W_0 (cm^3 g^{-1})**	**L (nm)**	**D (nm)**	**W_0 (cm^3 g^{-1})**	**L (nm)**
PSA-PA	0.61	671	0.37	0.27	1.44	1.11	0.28	1.58
GACN	0.65	629	0.75	0.27	-	2.38	0.30	1.71

V_p - total pore volume; W_0 - micropore volume; L - average micropore width; D - average pore diameter ($2V_p/S_{BET}$, assuming slit-shaped pores)

Table 6 – Fitting results of the kinetic and equilibrium models for the adsorption of CBZ, SMX and PAR from ultra-pure water and wastewater (STP effluent) onto PSA-PA and GACN.

		PSA-PA		GACN		PSA-PA		GACN		PSA-PA		GACN	
		CBZ				SMX				PAR			
		ultra-pure water	STP effluent	ultra-pure water	STP effluent	ultra-pure water	STP effluent	ultra-pure water	STP effluent	ultra-pure water	STP effluent	ultra-pure water	STP effluent
Kinetic models													
PFO	q_t	44 ± 1	14 ± 1	52 ± 2	22 ± 2	38 ± 3	4.3 ± 0.3	60 ± 3	20 ± 1	34 ± 3	20 ± 5	23 ± 3	21.0 ± 0.8
	k_1	(1.22 ± 0.08) x10^{-3}	(2.0 ± 0.6) x10^{-3}	(2.3 ± 0.2) x10^{-3}	(1.1 ± 0.3) x10^{-3}	(2.4 ± 0.6) x10^{-3}	(3.8 ± 0.8) x10^{-3}	(1.5 ± 0.2) x10^{-3}	(1.1 ± 0.2) x10^{-3}	(1.1 ± 0.3) x10^{-3}	(4 ± 2) x10^{-4}	(4 ± 1) x10^{-3}	(1.3 ± 0.1) x10^{-3}
	R^2	0.991	0.863	0.986	0.932	0.936	0.944	0.977	0.971	0.928	0.923	0.847	0.986
PSO	q_t	53 ± 2	15 ± 1	63 ± 4	26 ± 3	43 ± 5	4.8 ± 0.3	71 ± 4	24 ± 1	43 ± 7	31 ± 12	26 ± 5	26 ± 2
	k_2	(2.4 ± 0.2) x10^{-5}	(2.1 ± 0.9) x10^{-4}	(3.9 ± 0.8) x10^{-5}	(5 ± 2) x10^{-5}	(7 ± 3) x10^{-5}	(1.1 ± 0.3) x10^{-3}	(2.4 ± 0.5) x10^{-5}	(5 ± 1) x10^{-5}	(2 ± 1) x10^{-5}	(9 ± 10) x10^{-6}	(2 ± 1) x10^{-4}	(5 ± 2) x10^{-5}
	R^2	0.995	0.916	0.980	0.950	0.901	0.952	0.983	0.986	0.913	0.918	0.790	0.972
Isotherm models													
Langmuir	q_m	24 ± 5	10 ± 1	85 ± 14	Not Converged	44 ± 5	6 ± 1	98 ± 17	49 ± 6	31 ± 6	34 ± 9	64 ± 12	106 ± 40
	K_L	1.3 ± 0.8	0.5 ± 0.1	2.2 ± 0.9		0.6 ± 0.2	1 ± 1	0.6 ± 0.2	0.30 ± 0.06	0.6 ± 0.2	0.3 ± 0.1	0.6 ± 0.2	0.2 ± 0.1
	R^2	0.895	0.984	0.946		0.970	0.866	0.967	0.995	0.973	0.967	0.960	0.982
Freundlich	K_F	12 ± 2	3.2 ± 0.2	57 ± 3	12 ± 1	16 ± 1	3.2 ± 0.5	36 ± 3	10.6 ± 0.4	12 ± 1	8 ± 1	23 ± 3	19 ± 1
	n	3 ± 1	1.8 ± 0.2	2.4 ± 0.4	1.1 ± 0.1	1.9 ± 0.2	3 ± 1	1.6 ± 0.3	1.3 ± 0.1	1.7 ± 0.3	1.4 ± 0.2	2.0 ± 0.5	1.2 ± 0.1
	R^2	0.845	0.969	0.966	0.950	0.968	0.781	0.937	0.986	0.958	0.947	0.923	0.984
Sips	q_m	20 ± 4	8 ± 1	Ambiguous fitting	Ambiguous fitting	58 ± 45	5.0 ± 0.3	70 ± 10	Ambiguous fitting	18.5 ± 0.6	19 ± 2	43 ± 2	Ambiguous fitting
	K_S	2 ± 2	0.7 ± 0.2			0.4 ± 0.4	5 ± 4	1.3 ± 0.5		2.4 ± 0.4	0.8 ± 0.2	1.3 ± 0.2	
	N	0.6 ± 0.4	0.8 ± 0.2			1.2 ± 0.6	0.3 ± 0.1	0.6 ± 0.1		0.39 ± 0.04	0.5 ± 0.1	0.43 ± 0.06	
	R^2	0.905	0.986			0.971	0.959	0.979		0.998	0.982	0.996	

q_t – Amount of adsorbate removed at time *t* per unit mass of adsorbent (mg g^{-1}); k_1 – Rate constant of pseudo-first order (min^{-1}); k_2 – Rate constant of pseudo-second order (g mg^{-1} min^{-1}); **PFO** – Pseudo-first order model; **PSO** – Pseudo-second order model; q_e - Amount adsorbed at equilibrium (mg g^{-1}); C_e - Equilibrium concentration of the adsorbate (mg L^{-1}); q_m – Maximum adsorption capacity (mg g^{-1}); K_L – Equilibrium constant related with the free energy of adsorption (L mg^{-1}); K_F – Relative adsorption capacity ($mg^{1-1/n}$ $L^{1/n}$ g^{-1}); n – Constant related with the degree of non-linearity of the equation; K_S – Affinity coefficient of the Sips model (mg g^{1-} $(mg\ L^{-1})^{-1/N}$); N – degree of non-linearity of the Sips model.

Figure Captions

Figure 1 – Pore size distribution of PSA-PA and GACN.

Figure 2 – Scanning electron microscopy (SEM) images for PSA-PA and GACN at magnifications of 300x, 3000x, 10 000x and 50 000x.

Figure 3 – Kinetic experimental results and fittings to pseudo-first order (PFO, full line) and pseudo-second order (PSO, dashed line) kinetic models for the adsorption of CBZ, SMX and PAR onto PSA-PA (dots) and GACN (triangles) in ultra-pure water (full symbols) and in wastewater (open symbols). Note: Error bars stand for standard deviations (N = 3).

Figure 4 – Equilibrium experimental data and fittings to Langmuir (full line) and Freundlich (dashed line) isotherm models for the adsorption of CBZ, SMX and PAR onto PSA-PA (dots) and GACN (triangles) in ultra-pure water (full symbols) and in wastewater (open symbols). Note: Error bars stand for standard deviations (N = 3).

Figure 1

Click here to download high resolution image

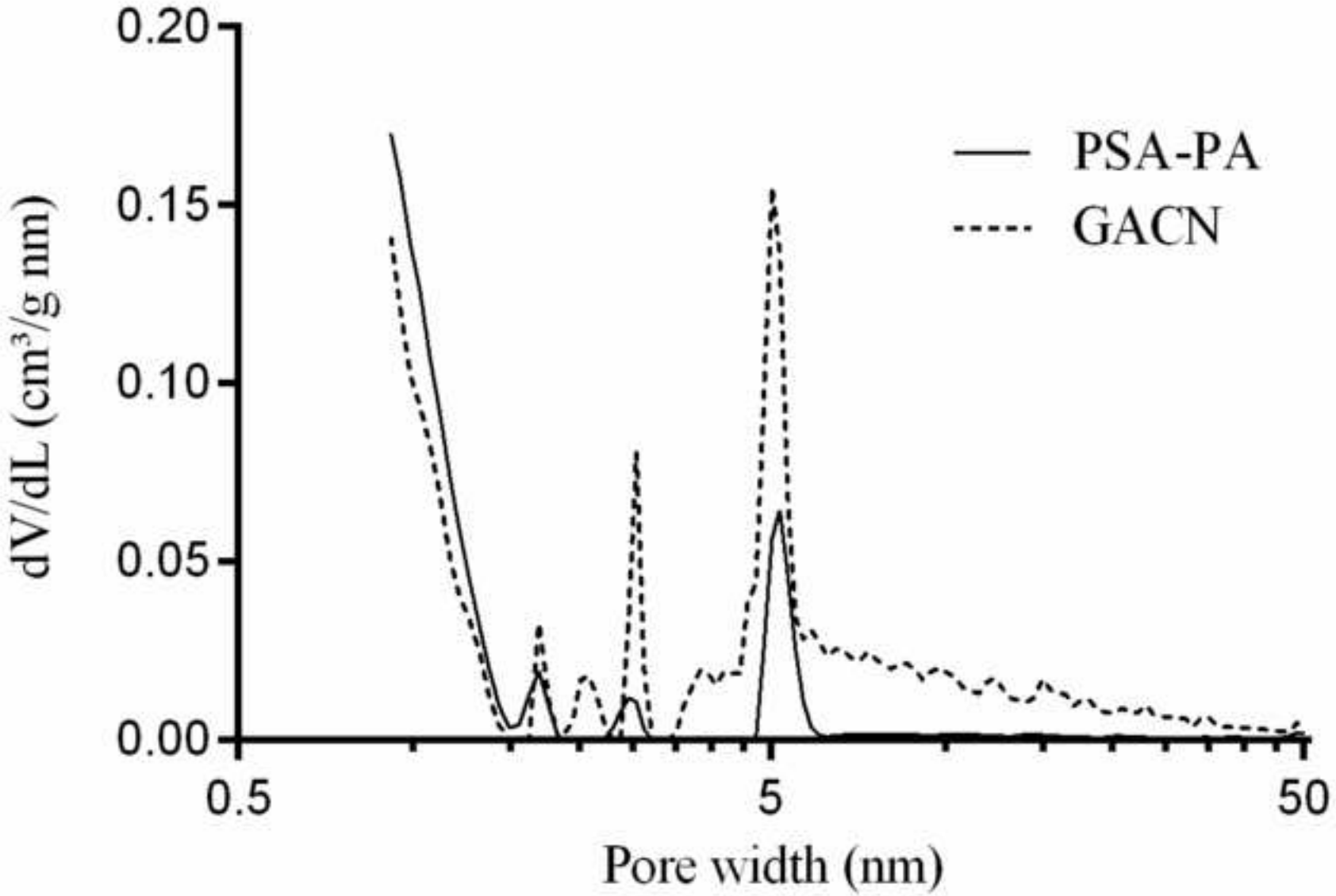

Figure 2

Click here to download high resolution image

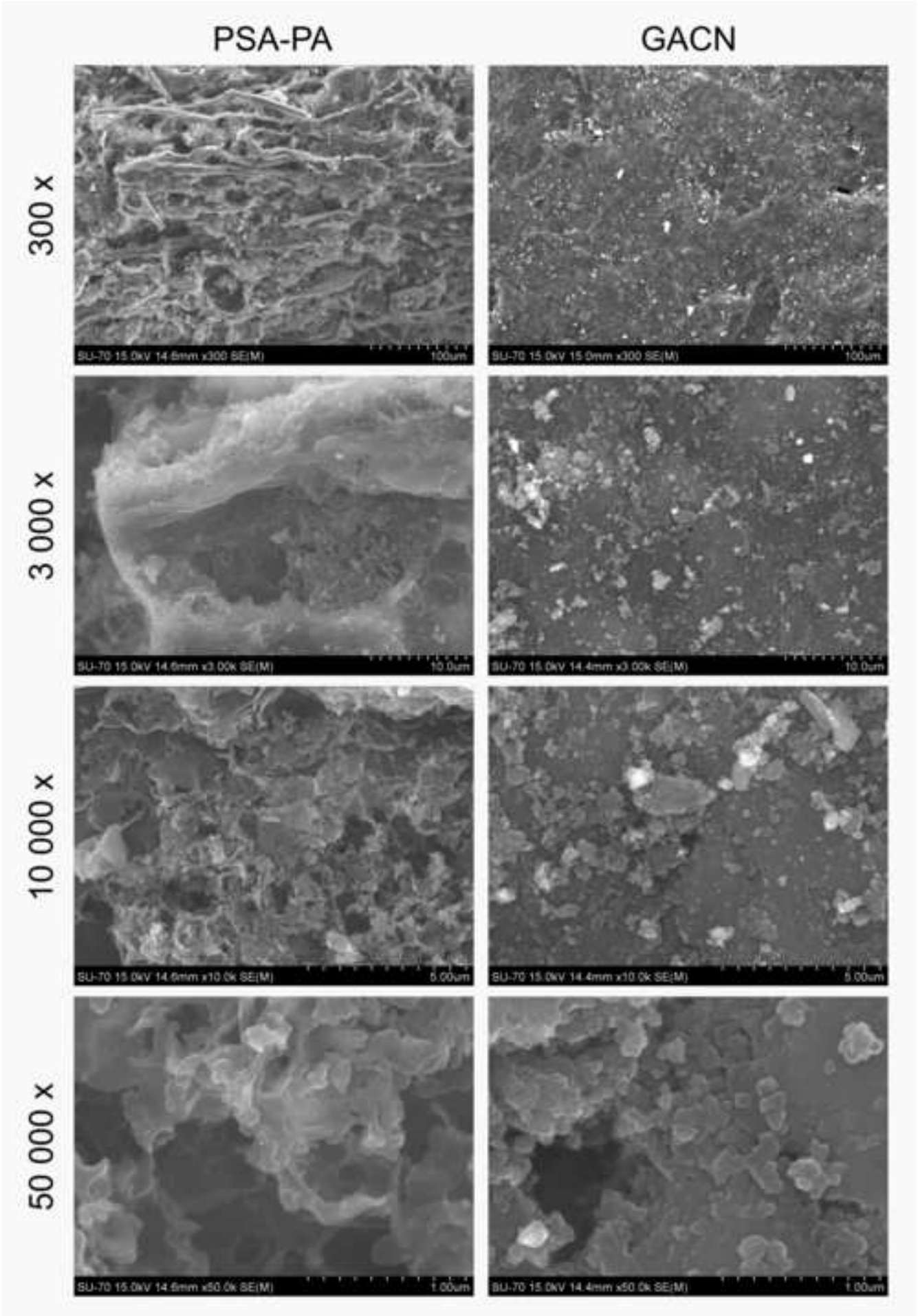

Figure 3 B&W

Click here to download high resolution image

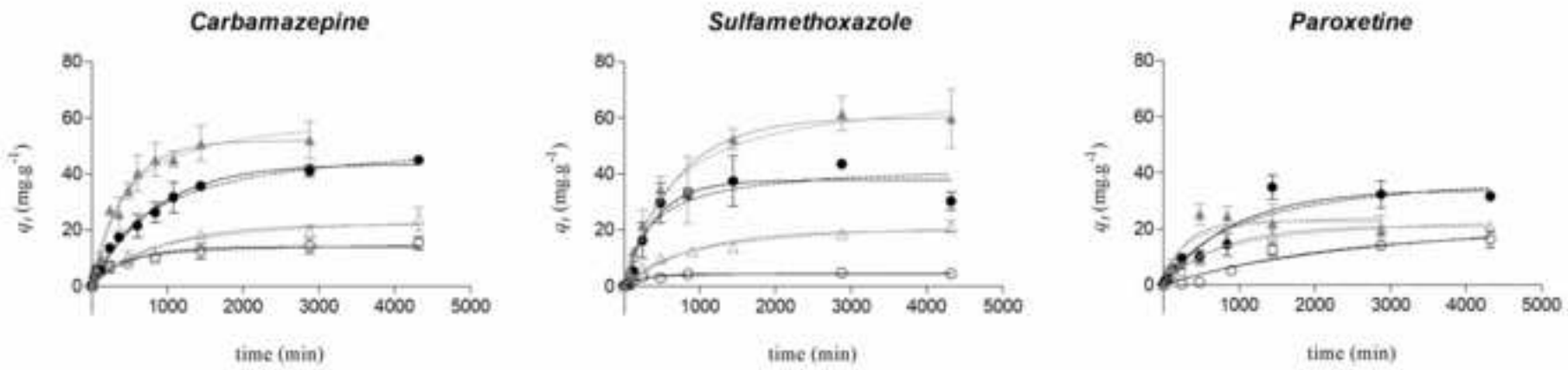

Figure 3 color

Click here to download high resolution image

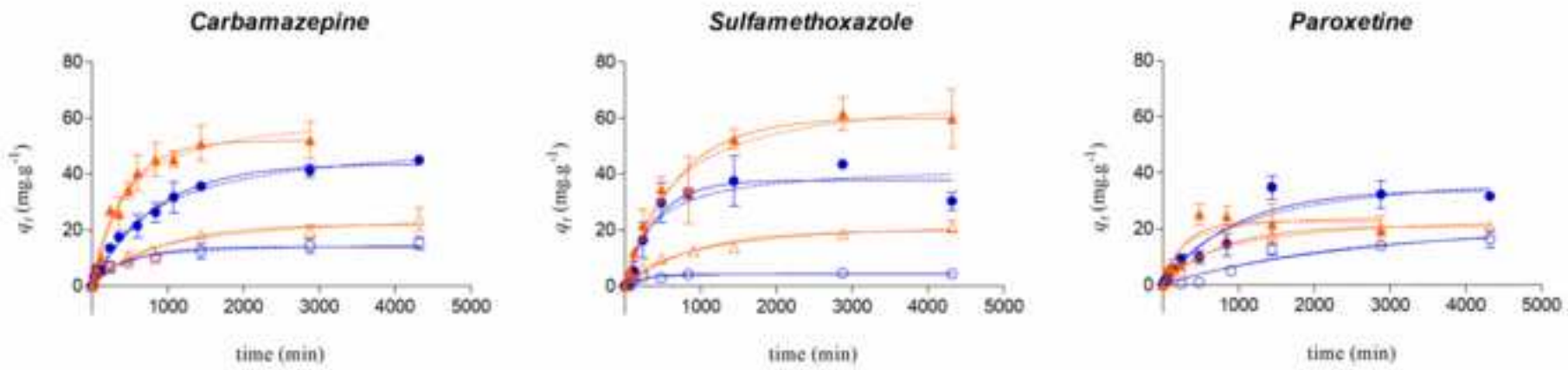

Figure 4 B&W

Click here to download high resolution image

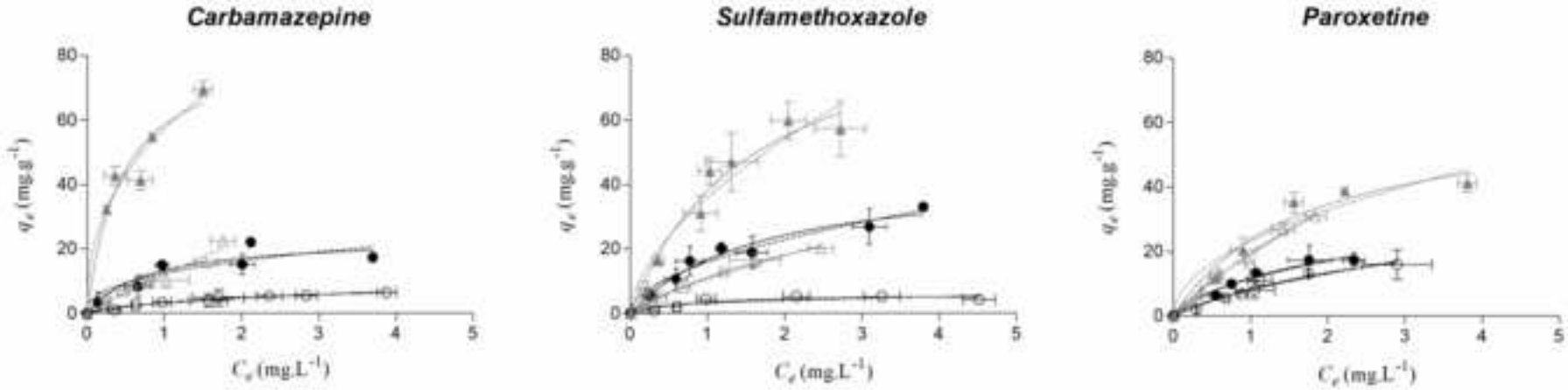

Figure 4 color

Click here to download high resolution image

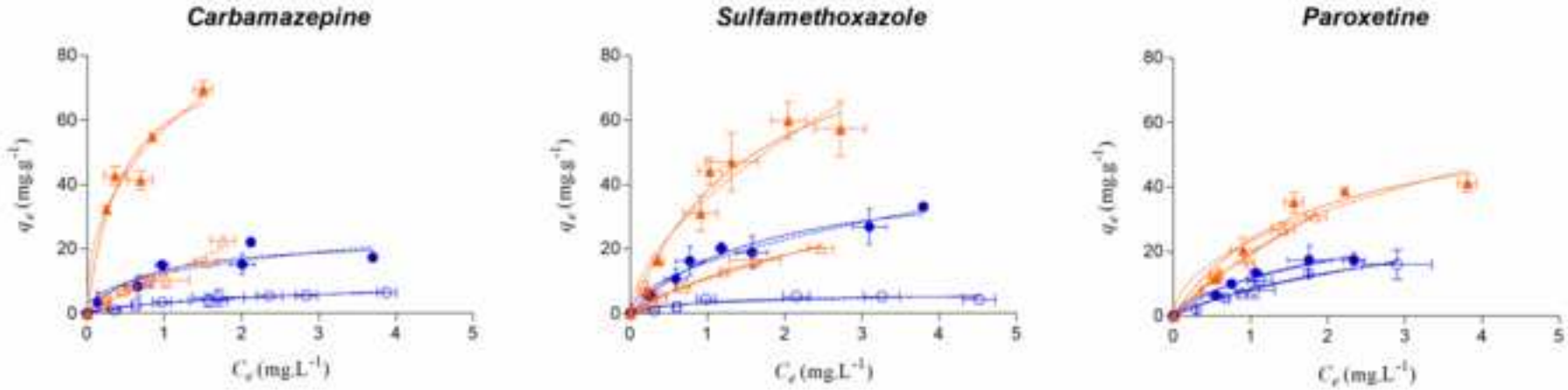

Supplementary material for on-line publication only

Click here to download Supplementary material for on-line publication only: supplementary material_REVISED.pdf